Kinetic formation of trimers and multimers in a spinless fermionic chain

Lorenzo Gotta,[1,*] Leonardo Mazza,[1] Pascal Simon,[2] and Guillaume Roux[1]
[1]*Université Paris-Saclay, CNRS, LPTMS, 91405 Orsay, France*
[2]*Université Paris-Saclay, CNRS, Laboratoire de Physiques des Solides, 91405 Orsay, France*

(Received 19 November 2021; revised 8 April 2022; accepted 11 April 2022; published 19 April 2022)

We study a chain of spinless fermions with a multimer hopping term which kinematically favors the formation of multimers and competes with single-particle hopping. We argue that this model generically stabilizes two different multimer phases, as well as intermediate phases where the free-fermion and multimer fluids coexist and do not spatially separate. Using density-matrix renormalization group techniques, we establish the phase diagram of the model in the case of trimers. For one of the intermediate phases, hybridization between the fermions and trimers liquids does occur and the onset of their correlations is well captured by a generalized BCS-like ansatz. The case of tetramers is finally addressed.

DOI: 10.1103/PhysRevB.105.134512

I. INTRODUCTION

Pairing of more than two particles to form multimers, is a transverse topic in physics, from nuclear and particle physics to condensed matter and cold-atom gases [1–4]. The first kind of multimers beyond pairs are naturally trimers, a three-body bound state. Beyond neutrons and protons made of three bound quarks, trimers have been widely discussed in the context of Efimov states [5–9] and in helium physics [10,11]. With the versatility of cold-atom platforms in terms of internal degrees of freedom and interactions, many proposals for trimers formation arose in the quantum matter literature, using spin-balanced [12–20] or spin-imbalanced fermionic mixtures [21–23], or fermions with different masses [24–26]. Signatures of bosonic trimers have also been discussed both in one [27–30], two [31–33], and three dimensions [34].

Forming trimers composed of a unique fermionic species—spin-polarized fermions—is particularly challenging despite seminal results in the context of the quantum Hall effect [35]. The pairing of spinless fermions already shows a rich phenomenology [36–46], and it is a crucial mechanism for some topological phases of matter, motivating further investigations in this direction. An intuitive route is to use attractive density interactions [43] on a chain and stabilize trimers using a third neighbor repulsion to prevent phase separation. In order to develop a low-energy description, as a trimer phase cannot be interpreted as an instability of the Luttinger liquid theory, the authors of Ref. [43] propose an emergent-mode description, which is then treated with bosonization tools. Unfortunately, such an approach is not conclusive on the nature of the transition from the Luttinger liquid to the trimer phase.

In this paper, instead of using interactions, we propose and study a simple microscopic model that realizes multimer and trimer phases thanks to a multimer-hopping term, extending the pairing mechanism foreseen in Ref. [41]. It contains tightly bound multimers and allows for a detailed study of the transitions between the fermionic and the multimer phases. On phenomenological grounds, it is also likely to support two two-fluid coexistence phases for which we derive the phase boundaries. Remarkably, the case of trimers does realize these two intervening phases in which a liquid of trimers spatially coexists with a liquid of unbound fermions. Our analysis generalizes the pioneering work of Ref. [42], where pairing physics is described with the help of two fictitious fluids of unpaired and paired fermions, a method that was successfully applied [45,46] to the model of Ref. [41]. The model we study here offers an exciting playground in which the trimer density and effective interaction with the unbound fermions is controlled by a single parameter. When the momenta of the trimers and of the unbound fermions in their respective Fermi seas are significantly displaced from each other in reciprocal space, the two fluids hardly interact. This corresponds to one of the intervening phases. However, when the Fermi sea of the unbound fermions and the one of the trimers overlap in reciprocal space, momentum-conserving processes turning fermions into trimers and vice versa take place. This occurs for the second intervening phase which is thus a correlated two-fluid phase. To capture such physics, we develop a generalized BCS wave function ansatz which encapsulates the coherent conversion between three fermions and a trimer and vice versa (we dubbed it the 3BCS ansatz as it involves trimers). Such ansatz well describes quantum correlations between the two fluids and also allows analytical calculations which qualitatively compare well with DMRG calculations. Finally, we turn to the case of tetramers formation. Although the phase diagram shares similar features with the pair and trimer cases, the intervening phases are extremely well described by the two-fluid model, supporting that the two fluids are almost uncorrelated.

The plan of the paper is as follows. In Sec. II we introduce our model Hamiltonian with a multimer correlated hopping term and our phenomenological and general two-fluid picture.

*lorenzo.gotta@universite-paris-saclay.fr

In Sec. III we specialize in trimers and present an extensive study of the phase diagram together with the intermediate phases where both liquids coexist. The 3BCS ansatz is introduced in this section. Section IV presents the study of the tetramers where we emphasize that the phenomenology becomes somehow simpler than for pairs and trimers. Finally, Sec. V presents a brief conclusion and summary of our results.

II. HAMILTONIAN AND TWO-FLUID PHENOMENOLOGY

A. Multimer model

We consider a chain of size L with N spinless fermions described by creation and annihilation operators $\hat{c}_j^{(\dagger)}$. In what follows, we choose a fermion density $n = N/L = 0.25$. We generalize the pair-hopping model of Ruhman and Altman [41] by introducing a multimer-hopping term t' competing with the single-particle hopping $t > 0$:

$$\hat{H} = -t\sum_j (\hat{c}_j^\dagger \hat{c}_{j+1} + \text{H.c.}) - t'\sum_j \hat{c}_j^\dagger \left(\prod_{m=1}^{M-1} \hat{n}_{j+m}\right)\hat{c}_{j+M} + \text{H.c.} \quad (1)$$

In order to highlight the physical meaning of the interaction term, Hamiltonian (1) is recast in the form

$$\hat{H} = -t\sum_j (\hat{c}_j^\dagger \hat{c}_{j+1} + \text{H.c.}) - (-1)^{M-1} t'\sum_j (\hat{M}_j^\dagger \hat{M}_{j+1} + \text{H.c.}), \quad (2)$$

where $\hat{M}_j = \hat{c}_j \hat{c}_{j+1} \cdots \hat{c}_{j+M-1}$ is the multimer operator. We have $M = 2$ for pairs (bosons), $M = 3$ for trimers (fermions), and $M = 4$ for tetramer (bosons), etc. For relative distances larger than M, the $\hat{M}_j$ operators commute or anticommute depending on their statistics. They also have a hard-core-like feature $\hat{M}_j^2 = 0$ but cannot be exactly mapped onto fermionic or hard-core bosonic operators due to their spatial extension. Models featuring $\hat{M}_j$ as the interaction term have been discussed, e.g., in the form of generalized Kitaev chains with even multiplet pairing fields [47], leading to the prediction of nontopological parafermions. For numerical calculations we compute the ground state properties of (1) using state-of-the-art density-matrix renormalization group (DMRG) simulations [48–51] implemented from the ITensor library [52].

B. $t' = 0$ and multimer formation

While $t' = 0$ is the free fermions limit, the $t = 0$ limit is also intuitive. Indeed, configurations that gain the most kinetic energy in a low-density picture are the ones with multimers, a multimer being M occupied neighboring sites surrounded by two empty sites. At the configurations level, this observation allows us to restrict the Hilbert space to configurations on which the Hamiltonian (1) can act to minimize energy. If one takes the examples of trimers, for which we use the label T, we assume that the ground state only explores the trimer subspace $\mathcal{H}_T$ spanned by Fock states with clusters of $3n$ fermions with integer n. For instance, $|\circ\bullet\bullet\bullet\circ\bullet\bullet\bullet\bullet\bullet\rangle$ belongs to $\mathcal{H}_T$, whereas $|\bullet\bullet\bullet\bullet\circ\circ\circ\bullet\circ\circ\bullet\bullet\rangle$ does not.

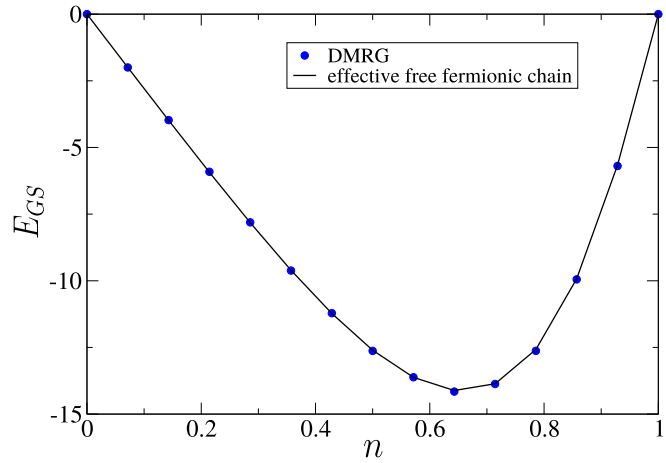

FIG. 1. DMRG ground state energy $E_{\text{GS}} = N\epsilon_{\text{GS}}$ for $M = 3$ and $L = 42$ sites with PBC with $t' = 1$ and $t = 10^{-4}$ as a function of the filling n and compared with the analytical expression provided in Eq. (3).

Regardless of the value of M, the energy will be that of a one-dimensional band filled with $N_M = N/M$ multimers. Effectively, due to excluded volume effects, the center-of-mass of multimers live over a lattice of size $L - (M-1)N_M$. The band dispersion of the multimers is given by $\varepsilon_M(k) = (-1)^M 2t'\cos(k)$, in which the sign depends on the statistics. The minimum either lies $k_0 = 0$ ($t' > 0$ for trimers) or at $k_0 = \pi$ ($t' < 0$ for trimers). The Fermi points are located at $k_0 \pm \pi\frac{N_M}{L-(M-1)N_M}$. Consequently and at a phenomenological level we thus expect the ground state energy density $\epsilon_{\text{GS}} = E_{\text{GS}}/N$ to follow:

$$\epsilon_{\text{GS}} = -\frac{2|t'|}{\pi}\left(1 - \frac{(M-1)n}{M}\right)\sin\left(\frac{\pi n}{M-(M-1)n}\right). \quad (3)$$

The prediction of Eq. (3) is compared to numerical results in Fig. 1. The result as a function of the filling n of the system shows an excellent agreement. We perform DMRG simulations on a system of size $L = 42$ in PBC for $t' = 1$ and $t = 10^{-4}$. A nonvanishing but negligible value of t is used to allow the DMRG algorithm to converge to the ground state of the system irrespectively of the initial state.

C. The two-fluid picture

When both terms are competing, a simple picture is that the system forms a mixture of a free fermions fluid and of a multimers fluid, whose densities are adjustable to minimize the total energy. Such an ansatz gave remarkably good predictions for $M = 2$ and $t'/t > 0$ [45,46]. Assuming the two fluids are noninteracting, the two-fluid model (2F) Hamiltonian splits into

$$\hat{H}_{\text{2F}}^{(M)} = \sum_k \varepsilon_F(k)\hat{a}_k^\dagger \hat{a}_k + \sum_k \varepsilon_M(k)\hat{d}_k^\dagger \hat{d}_k, \quad (4)$$

where $\varepsilon_F(k) = -2t\cos k$ is the free fermion dispersion relation associated with unbound fermions operators $\hat{a}_k$. The $\hat{d}_k$ are fermionic or bosonic effective multimer operators. Nor

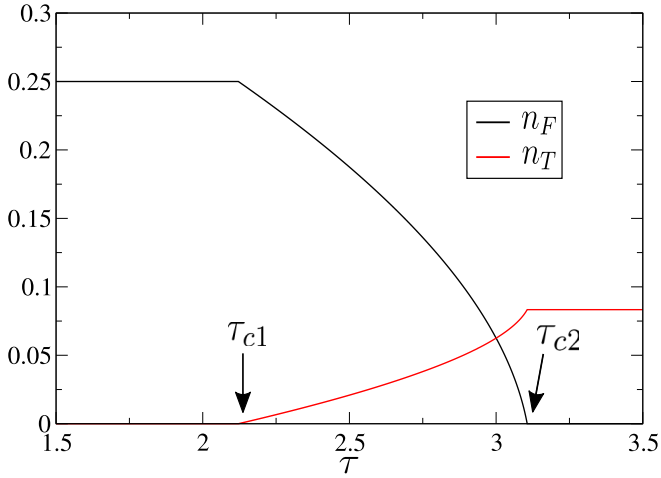

FIG. 2. Optimal fermionic density n_F and trimer density n_T as a function of $\tau = |t'/t|$ obtained by minimizing the total energy $\langle \hat{H}^{(3)}_{2F} \rangle$ for a density $n = 0.25$. We observe (i) the F phase ($n_F = n$) for $\tau < \tau_{c1} \simeq 2.12$, (ii) the T phase ($n_F = 0$) for $\tau > \tau_{c2} \simeq 3.11$, and (iii) the TF-C phase ($0 < n_F < n$) for $\tau_{c1} < \tau < \tau_{c2}$.

the $\hat{a}_k$ or the $\hat{d}_k$ have any exact connection with the lattice operators $\hat{c}_j$. Note that, in this typically low-density approximation, we neglect excluded volume effects. Since the total number of particles is fixed, the unbound fermions density n_F and the multimer density n_M must satisfy the constraint $n_F + M n_M = n$. The evolution of the densities $n_{F,M}$ when increasing $\tau = |t'/t|$ is obtained by minimizing the total energy of Hamiltonian (4) under this constraint.

We present in Fig. 2 the general structure of the resulting phase diagram for the case $M = 3$ by showing the fermionic density profile n_F and the trimer density profile n_T as a function of τ. At small values of τ we find a purely fermionic region (F phase) with $n_F = n$ and $n_M = 0$. At large values of τ, we find a purely multimer region (trimer T phase) with $n_F = 0$ and $n_M = n/M$. In between, there exists an intervening coexistence phase of fermions and multimers with $0 < n_F < n$ and $0 < n_M < n/M$ (the MF-C phase) such that both bands are partially filled.

In order to determine the phase boundaries of the MF-C phase, we consider the minimization condition determining the optimal fermionic density, namely,

$$\cos(\pi n_F) = \frac{\tau}{M} \cos\left(\pi \frac{n - n_F}{M}\right). \tag{5}$$

The first transition point τ_{c1} separating the F phase from the MF-C phase is obtained by taking the limit $n_F \to n$ in Eq. (5), which gives $\tau_{c1}^{(M)} = M \cos(\pi n)$. With $n = 1/4$, the values for $M = 3$ and $M = 4$ are, respectively, $\tau_{c1}^{(3)} \simeq 2.12$ and $\tau_{c1}^{(4)} \simeq 2.83$. Similarly, the critical point τ_{c2} separating the MF-C phase from the M phase is obtained from the limit $n_F \to 0$ in Eq. (5) and gives $\tau_{c2}^{(M)} = M/\cos(\frac{\pi n}{M})$. The two predictions for $M = 3$ and $M = 4$ are, respectively, $\tau_{c2}^{(3)} \simeq 3.11$ and $\tau_{c2}^{(4)} \simeq 4.08$.

We underline that, at the level of the noninteracting two-fluid Hamiltonian (4), the behavior of the densities $n_{F,M}$ is identical for both positive and negative values of t'. However,

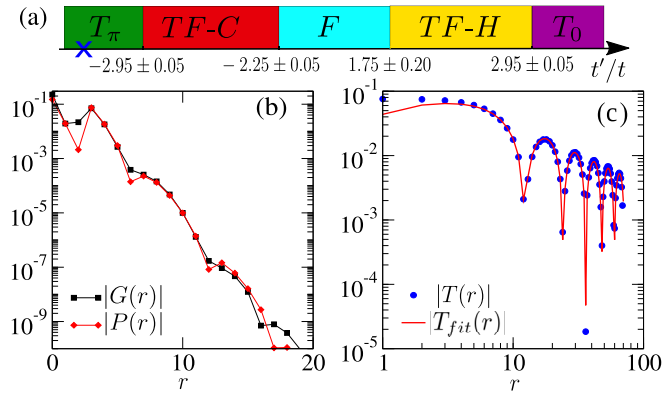

FIG. 3. (a) Phase diagram of the model in Eq. (1) (not in scale). (b) and (c) Correlators for $t'/t = -3.5$ [blue cross in (a)]: $G(r)$ for single-particle, $P(r)$ for pairs (both exponential), $T(r)$ for trimers (algebraic), and $T_{\rm fit}(r)$ for the fitting function of trimer two-point correlators.

it is known that, e.g., for $M = 2$ [45,46], this approach provides a rather good account of the phase diagram for $t' > 0$ but not for $t' < 0$, because of the difference in the scattering between unpaired fermions and pairs. The parameter regimes where interspecies interactions introduce deviations from the phenomenology presented in Fig. 2 will thus be highlighted in the following sections.

III. TRIMER FORMATION AND TRIMER-FERMION MIXTURES

We now focus on the actual phase diagram of Hamiltonian (1) in the case of trimers $M = 3$ and for which we rather use the label T instead of M.

A. Phase diagram

We denote by $\hat{T}_j = \hat{c}_j \hat{c}_{j+1} \hat{c}_{j+2}$ the trimer operator, keeping in mind that they are almost fermions. In order to systematically probe the phase diagram summarized in Fig. 3(a), we compute local observables and the single-particle, pair and trimer two-point correlators

$$G(r) = \langle \hat{c}_j^\dagger \hat{c}_{j+r} \rangle, \quad P(r) = \langle \hat{P}_j^\dagger \hat{P}_{j+r} \rangle, \quad T(r) = \langle \hat{T}_j^\dagger \hat{T}_{j+r} \rangle,$$

with $\hat{P}_j = \hat{c}_j \hat{c}_{j+1}$. When $t'/t = -3.5$, Figs. 3(b) and 3(c) show clear evidence for a trimer phase: the trimer correlator $T(r)$ displays an algebraic decay, whereas single-particle and pair correlators $G(r)$ and $P(r)$ decay exponentially. Moreover, the single-particle and pair correlation lengths coincide. This reflects the existence of both single and two-particle gaps, while the three-particle excitations remain gapless. The $t' > 0$ and $t' < 0$ phases have a different nature and are respectively denoted by T_0 and T_π as we will see. The fit in Fig. 3(c) of $T(r)$ to the modulated algebraic decay $T_{\rm fit}(r) = A \frac{\cos(kr+\varphi)}{r^\alpha}$ (A, k, φ, and α being fit parameters) shows that the effective Luttinger liquid behavior of the trimer fluid is that of almost free fermions with algebraic decay exponent $\alpha \simeq 1$ and oscillations at $k_T = \pi n_T$. The $t' = 0$ free fermions point extends in a regular fermionic Luttinger-liquid phase F in which all correlators are algebraically decaying. The analysis

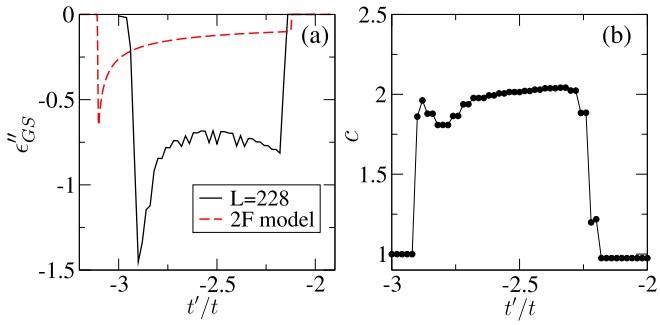

FIG. 4. (a) Second derivative of the ground state energy density $\epsilon''_{\rm GS}$ with respect to t'/t for the Hamiltonian in Eq. (1) (continuous line) and for the model $\hat{H}_{\rm 2F}$ (dashed line). (b) Central charge c as a function of t'/t.

of the energy density and its derivatives as a function of t'/t allows us to find the boundaries of these five different phases: the two coexistence phases appear for $-2.95 \pm 0.05 < t'/t < -2.25 \pm 0.05$ and $1.75 \pm 0.20 < t'/t < 2.95 \pm 0.05$.

As regards the two intermediate phases TF-C and TF-H, they show two kinds of coexistence phases between trimers and fermions. The TF-H coexistence phase is a phase in which trimers and unbound fermions significantly interact, so we postpone its analysis to Sec. III C. On the contrary, the TF-C is already well interpreted by the two-fluid model. In Fig. 4(a) we compare the behavior of the second derivative of the energy density computed using $\hat{H}_{\rm 2F}$ with the one obtained from ground state DMRG simulations for the Hamiltonian (1). They agree qualitatively well, and almost quantitatively for the transition points, despite the simplicity of the 2F ansatz. In addition, the numerical calculation of the central charge c gives $c = 2$ for TF-C and $c = 1$ for T_π and F, as shown in Fig. 4(b). This probes the number of gapless modes of the system and further supports the proposed two-fluid interpretation. We thus conclude that two Lifshitz transitions characterized by a nonperturbative reshaping of the Fermi points separate the three phases for $t' < 0$.

The remarkable agreement shows that the residual interaction between unbound fermions and trimers is negligible, so that the two fluids hardly hybridize. The reason is that the fermionic and trimer Fermi seas are significantly displaced in momentum space. Any interaction process responsible for turning a trimer into three fermions (or vice versa) must conserve the lattice momentum, which makes the process extremely unlikely. At most, density-density interactions between fermions and trimers might only shift the locations of the phase boundaries.

B. Fourier transform of the density profile

We analyze the behavior of the Fourier transform of the density profile in the parameter regions where the transition from T_π and T_0 phases to the F phase takes place, respectively. The result, presented in Figs. 5(c) and 5(d), shows that the behavior in the two cases is qualitatively similar.

In the fermionic phase, a peak at $k = 2\pi n$ is observed, in agreement with the Luttinger liquid prediction

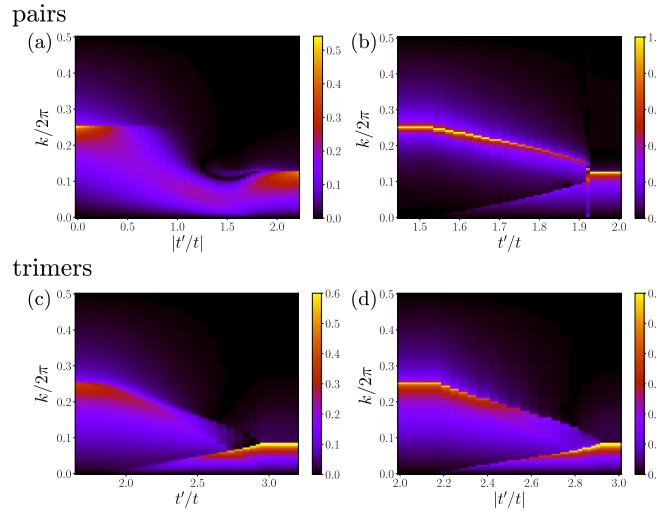

FIG. 5. (a) and (b) Fourier transform of the density profile in the ground state of the model with correlated pair hopping studied in [44,45] for $t'/t < 0$ (a) and $t'/t > 0$ (b). (c) and (d) Fourier transform of the density profile in the ground state of the model defined in Eq. (1) of the main text for $t'/t > 0$ (c) and $t'/t < 0$ (d).

of the wave vector associated with the leading modulation in the density fluctuations. Similarly, in the trimer phase, the effective Luttinger liquid density is $n_T = n/3$ due to trimer formation, thus resulting in a leading peak at $k = 2\pi n_T$.

The situation is richer in the intermediate phase separating the two aforesaid limits. We first observe a peak interpolating between the one in the F phase and the one in the T_π and T_0 phases. This observable is actually a way to track the effective densities of fermions n_F and trimers n_T. This signal can be interpreted as the leading density modulation in a Luttinger liquid phase at density $n_F + n_T$ where both uncoupled fermions and trimers populate the lattice. The peak is less sharply defined close to the transition from the F phase to the TF-H phase, where the two species are strongly hybridized. Consistently with the picture of a coexistence between uncoupled fermions and trimers, we additionally observe a peak due to trimer formation at $k = 2\pi n_T$. One also observes a subleading peak at $k = 2\pi n_F$ which goes to zero when entering the T_π and T_0 phases.

For completeness we provide in Figs. 5(a) and 5(b) the same quantity for the ground state of the Hamiltonian (1) with $M = 2$ studied in Refs [45,46], whose interaction term implements correlated pair hopping processes. For $t'/t > 0$, a coexistence phase between paired and unpaired fermions is observed. If we denote the effective pair density as n_P, it results in the appearance of two distinct peaks at $k = 2\pi(n_F + n_P)$ and $k = 2\pi n_P$, together with a subleading one at $k = 2\pi n_F$. On the other hand, when $t'/t < 0$, a critical point belonging to the Ising universality class separates the F phase from a Luttinger liquid of pairs. The latter originates as a result of relevant pair-fermion interactions in an effective two-fluid description. Thus, it is not possible to observe an extended parameter region featuring well-defined peaks associated with effective gapless modes for pairs and unpaired fermions, respectively.

C. A BCS-like approach for the transition from T_0 to F

Since both bands minima are at $k = 0$ for $t' > 0$, the study of the transition from the F phase to the T_0 phase is more challenging. In this case, the two Fermi seas are overlapping and momentum-conserving processes turning fermions into trimers (and vice versa) can take place. We need to include in the Hamiltonian a new term such that $\hat{H}_{2F} = \hat{H}_F + \hat{H}_T + \hat{H}_{\rm int}$. To model the interaction, we consider a recombining term $\hat{H}_{\rm int} = g\sum_j d_j^\dagger \hat{a}_{j-1}\hat{a}_j\hat{a}_{j+1} + \text{H.c.}$ The value of the parameter g is introduced on a purely phenomenological basis.

We propose an approach based on a BCS-like ansatz wave function that we dub the 3BCS ansatz, which aims at capturing the emergence of the trimers. First, we introduce $|n_F\rangle$ as the Fermi sea state with fermionic density $n_F = n$ and Fermi momentum $k_F = \pi n$. Concerning trimers, we start from the vacuum $|v_T\rangle$. Our ansatz wave function reads

$$|\Psi_3\rangle = \prod_{-\frac{k_F}{3}<k<\frac{k_F}{3}} (\alpha_k + \beta_k \hat{d}_k^\dagger \hat{a}_{-k_F+\delta_k}\hat{a}_k\hat{a}_{k_F-\delta_k})|n_F\rangle\otimes|v_T\rangle, \qquad (6)$$

where $\delta_k = 2k$ for $k \geqslant 0$ and $\delta_k = -2k - 2\pi/L$ for $k < 0$. The wave function interpolates from the fermionic limit $\beta_k = 0$ to the trimer phase limit $\alpha_k = 0$. In the former case, the state reduces to $|n_F\rangle \otimes |v_T\rangle$, while in the latter case, trimers form a Fermi sea with Fermi momentum $k_T = \pi n/3$ and the fermionic system is empty. When both α_k and β_k are different from zero, $|\Psi_3\rangle$ includes quantum correlations between fermions and trimers: the creation of a trimer with momentum k is accompanied by the annihilation of three fermions at momenta k and $\sim \pm(k_F - 2|k|)$. This choice is motivated by a minimization calculation showing that in order to create a trimer with momentum $k = 0$, the most favorable choice is to annihilate three fermions at $k = 0$ and $k = \pm k_F$ (see Appendix 1 for a detailed discussion). The ansatz (6) thus captures some physically relevant forms of quantum correlations between the two fluids, and satisfies momentum conservation in the trimer-fermion exchange process. In addition, $|\Psi_3\rangle$ offers the advantage of being entirely composed of commuting terms (like the standard BCS wave function) and is thus well suited for analytical calculations.

By virtue of the normalization condition $|\alpha_k|^2 + |\beta_k|^2 = 1$, we introduce the parametrization $\alpha_k = \cos\theta_k$ and $\beta_k = e^{i\varphi_k}\sin\theta_k$, with $\theta_k \in [0, \pi]$ and $\varphi_k \in [0, 2\pi[$. We compute the expectation value of the Hamiltonian $\hat{H}_{2F}$ in state $|\Psi_3\rangle$. Defining $\epsilon_{\rm GS} = \frac{\langle \hat{H}_{2F}\rangle - E_{FS}}{Lt}$, where E_{FS} is the energy of the fermionic Fermi sea filled up to momentum k_F, we obtain

$$\epsilon_{\rm GS} = 2\int_0^{\frac{k_F}{3}} [A_k \sin^2\theta_k - B_k \sin 2\theta_k \sin\varphi_k]\frac{dk}{2\pi}, \qquad (7)$$

where

$$A_k = 2(1 - t'/t)\cos k + 4\cos(k_F - 2k),$$

$$B_k = \frac{2g}{Lt}[\sin(k_F - k) + \sin(4k - 2k_F) + \sin(k_F - 3k)].$$

Minimizing the functional (7) yields the solutions

$$\theta_k = \frac{1}{2}\arctan\left(\frac{2B_k}{A_k}\right) + \frac{\pi}{2}\Theta(-A_k), \quad \varphi_k = \frac{\pi}{2}, \qquad (9)$$

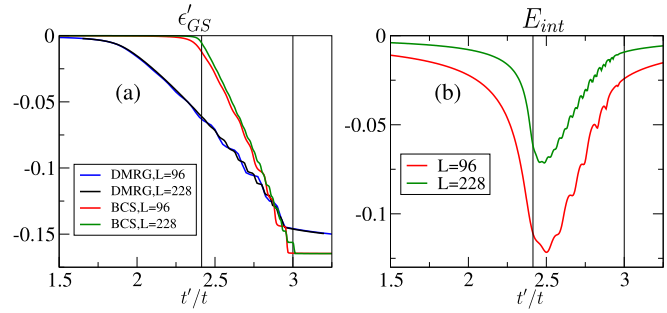

FIG. 6. (a) First derivative of the ground state energy density $\epsilon'_{\rm GS}$ with respect to t'/t from DMRG and the 3BCS ansatz with $g/t = 8$. (b) Interaction energy $E_{\rm int}$ for the 3BCS ansatz using $g/t = 8$. Vertical lines are transition points predicted by the 3BCS model.

where $\Theta(x)$ is the Heaviside step function. The plot of the first derivative of the ground state energy density obtained with the 3BCS ansatz is shown in Fig. 6(a), where we compare it with DMRG simulations of the Hamiltonian (1). By taking $g = 8t$, we reproduce correctly the numerical results obtained with $L = 96$ and $L = 228$, apart from a quantitative mismatch in the first transition point.

The 3BCS ansatz reproduces two important features of the numerical $\epsilon'_{\rm GS}$ curve: first, the steplike behavior appearing close to the T_0 phase and, second, the smoother profile close to the F phase. The first is a finite size effect that originates from the absence of a strong fermion-trimer hybridization: each step corresponds to the formation of a trimer. The second is naturally associated with the fermion-trimer recombination processes, which are here strongly relevant. This is further supported by the behavior of the fermion-trimer interaction energy $E_{\rm int} = -\frac{L}{\pi}\int_0^{\frac{k_F}{3}} B_k \sin 2\theta_k dk$ plotted in Fig. 6(b). We observe that the steplike behavior coincides with the weakly interacting region, whereas the smoother one is associated with strong interactions. Strictly speaking, the 3BCS ansatz gives an interaction energy $E_{\rm int}$ that scales to zero in the thermodynamical limit (see Appendix 7), as seen in Fig. 6(b). Yet, we believe that both in the DMRG and in the exact solution of H_{2F}, a residual hybridization remains relevant in the thermodynamical limit. The above considerations motivate the wording *trimer-fermion hybrid phase* (TF-H) for a phase that displays relevant hybridization processes at low trimer density on finite size systems and likely in the thermodynamical limit.

D. Occupation factors

To further support the relevance of the hybridization processes and their description with the 3BCS ansatz, we introduce "isolated" operators

$$\hat{F}_j^{(M)} = (1 - \hat{n}_j)\left(\prod_{m=1}^{M}\hat{c}_{j+m}\right)(1 - \hat{n}_{j+M+1}) \qquad (10)$$

that capture unbound fermions ($M = 1$) and isolated trimers ($M = 3$). Using DMRG, we can access the momentum

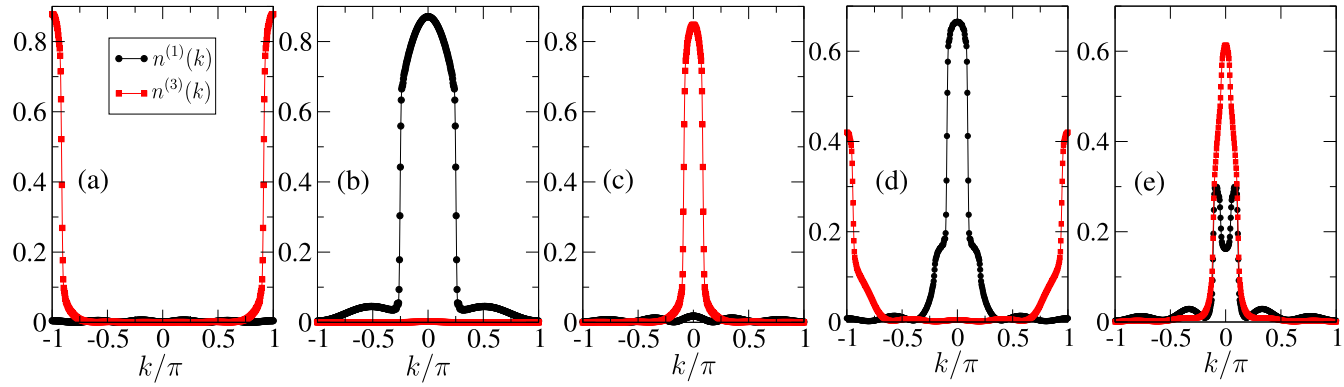

FIG. 7. Momentum distribution $n^{(1)}(k)$ and $n^{(3)}(k)$ with OBC and $L = 96$ in (a) the T_π phase for $t'/t = -3.5$, in (b) the F phase for $t'/t = 1.0$, in (c) the T_0 phase for $t'/t = 3.5$, in (d) the TF-C phase for $t'/t = -2.7$, and in (e) the TF-H phase for $t'/t = 2.9$.

distribution, or occupation factors

$$n^{(M)}(k) = \sum_{j,j'} e^{-ik(j-j')} \langle \hat{F}_j^{(M)\dagger} \hat{F}_{j'}^{(M)} \rangle \tag{11}$$

associated with each two-point correlators.

As an illustration for the relevance of these operators to describe the physics, we show in Figs. 7(a)–7(c) the unbound fermion and trimer momentum occupation functions, $n^{(1)}(k)$ and $n^{(3)}(k)$, respectively, in the T_π, T_0, and F phases. The two trimer phases feature a negligible $n^{(1)}(k)$ profile together with a quasicondensate around $k = \pi$ ($k = 0$) in the trimer occupation profile $n^{(3)}(k)$. On the other hand, the F phase shows a standard Fermi sea of unbound fermions around $k = 0$ in $n^{(1)}(k)$ and a vanishing $n^{(3)}(k)$ profile. These results are in striking agreement with the effective two-fluid approach adopted in the analysis of the phase diagram, as they give direct evidence for the band filling picture of unbound fermions and trimers.

In Figs. 7(d) and 7(e) the momentum distributions fully agree with the two-band picture and highlight the main differences between the TF-C and TF-H phases. In the latter case, the unbound fermion distribution in black displays a remarkable hollow around $k = 0$. Such a feature is perfectly coherent with the structure of the 3BCS ansatz, according to which the filling of the trimer states around $k = 0$ occurs via the annihilation of fermions around $k = 0$ and $k = \pm k_F$. While the fermionic occupation function is expected to develop a minimum at $k = 0$, its trimer counterpart gets maximal at $k = 0$. This feature is more visible close to the T_0 phase, where the transition is sharp and the trimer density higher, and less visible close to the F phase.

IV. TETRAMER FORMATION AND HYBRIDIZATION

Lastly, we extend the analysis to the phase diagram of Hamiltonian (1) for tetramers with $M = 4$. As in the trimer case, we find a standard F phase when $|t'| \ll t$ and two tetramer M phases with quasi-long-range-ordered tetramer correlator $M(r) = \langle \hat{M}_j^\dagger \hat{M}_{j+r} \rangle$ and exponentially decaying $G(r)$, $P(r)$, and $T(r)$.

In order to discuss the nature of the transition and the comparison with the 2F model, we present in Figs. 8(a) and 8(b) the first derivative of the ground state energy density, the total single-particle kinetic energy density

$$K_1 = \frac{1}{L} \sum_j \langle \hat{c}_j^\dagger \hat{c}_{j+1} + \text{H.c.} \rangle, \tag{12}$$

and the total tetramer kinetic energy density

$$K_4 = \frac{1}{L} \sum_j \langle \hat{M}_j^\dagger \hat{M}_{j+1} + \text{H.c.} \rangle. \tag{13}$$

Superimposing the curves obtained for $t'/t < 0$ and $t'/t > 0$ shows a remarkable quantitative agreement. We conclude that the two transitions have the same properties, differently from what has been found for pairs and trimers [41,45,46].

In Fig. 8(a) the comparison of the DMRG data with the 2F model predictions shows an excellent agreement. Accordingly, two Lifschitz transitions separate the coexistence phase from the fermionic phase and the tetramer phase. The numerical data also indicate that the effective interactions between the two fluids are thus strongly suppressed, even when the tetramers quasicondense at $k = 0$ for $t' < 0$. A first qualitative argument that supports this observation is that the larger the molecule, the higher is the order in perturbation theory to split it into M unbound fermions. Another one is an heuristic argument supporting an emergent $t' \to -t'$ symmetry in the Hamiltonian. Indeed, by highlighting the dependence of

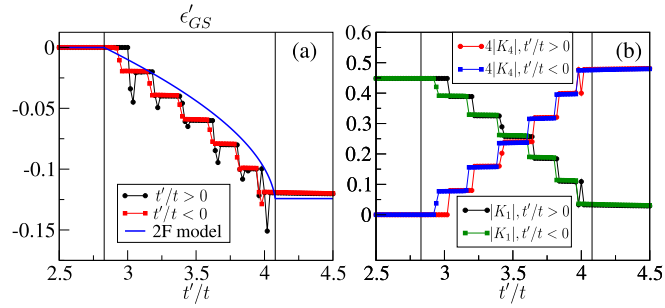

FIG. 8. Energy observables in the ground state of (1) with $M = 4$ on a lattice with $L = 96$ sites as a function of $|t'/t|$ for both $t' \geqslant 0$ and $t' \leqslant 0$. Vertical lines are transition points predicted by the generalized two-fluid model. (a) First derivative of the energy density with respect to t'/t from DMRG and two-fluid model. (b) Single-particle and tetramer kinetic energy densities $|K_1|$ and $4|K_4|$.

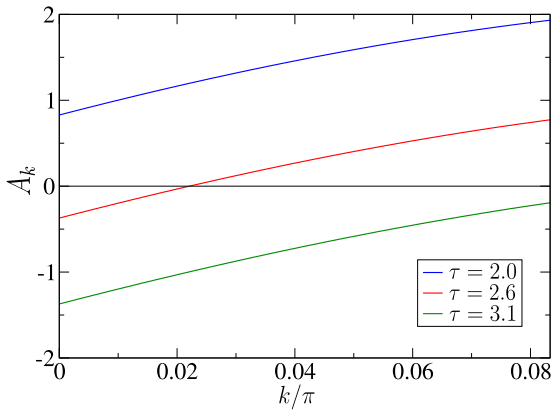

FIG. 9. A_k as a function of k for $\tau < \tau_1$ (blue curve), $\tau_1 < \tau < \tau_2$ (red line), and $\tau > \tau_2$ (green line).

Hamiltonian (1) on the multimer size M, t, and t' via $\hat{H} \equiv \hat{H}_M(t, t')$, we see that the unitary transformation $\hat{c}_j \to e^{i\frac{\pi}{M}j}\hat{c}_j$ transforms $\hat{H}_M(t, t')$ into $\hat{H}_M(e^{i\frac{\pi}{M}}t, -t')$. In the limit of large molecules $M \to +\infty$, the phase factor multiplying t tends to 1, connecting $\hat{H}_M(t, t')$ to $\hat{H}_M(t, -t')$. Since the coexistence phase is the generic scenario at low density when molecules quasicondense at $k = \pi$, the same is expected for quasicondensation at $k = 0$ on the opposite side.

V. CONCLUSIONS

In this paper we have studied the ground state phase diagram of a one-dimensional lattice model of spinless fermions with multimer hopping, focusing on the case of trimers. By means of an effective two-fluid model and numerical simulations, two remarkable coexistence phases are found, with one in which hybridization between unbound fermions and trimers is well described by an effective BCS ansatz. This scenario is generalized and becomes generic for a class of Hamiltonian with a hopping of arbitrarily large molecules. This scenario occurs for densities that are not too large. Intuitively, a higher density n will increase hybridization and could even open the path to new phases.

In the context of bound states formation with spinless fermions, the success of our interacting two-fluid approach provides a new set of interpretative ideas and technical tools that are expected to shed further light on the properties of experimentally relevant Hamiltonians for which multimer formation has been predicted [43]. The possibility of having a direct transition between fermionic and trimer phases remains an open question in these models.

ACKNOWLEDGMENT

This work has benefited from the financial support Investissements d'Avenir du LabEx PALM (ANR-10-LABX-0039-PALM). This work has been supported by Region Ile-de-France in the framework of the DIM Sirteq.

APPENDIX: DETAILS OF CALCULATIONS FOR THE 3BCS MODEL

1. Optimal fermion-trimer recombination process

We now consider a Fermi sea of unpaired fermions with Fermi edges at $k = \pm\pi n$ and study the formation of a trimer with momentum $k = 0$ via a momentum-conserving process of annihilation of three fermions and creation of a trimer. We prove that the optimal way of creating a trimer with momentum $k = 0$, i.e., at the bottom of the trimer band, via annihilation of three fermions from a Fermi sea is realized when the the latter have momenta $k = 0, \pm k_F$, where $k_F = \pi n$ is the Fermi momentum. To this goal we need to determine a triplet of momenta $(k_1, k_2, k_3) \in [-\pi n, \pi n]^3$ satisfying $\sum_{i=1}^{3} k_i = 0$ such that the total energy loss $-2t\cos k_1 - 2t\cos k_2 - 2t\cos k_3$ due to the annihilation of fermions at momenta k_1, k_2, k_3 is maximal. By symmetry we can always assume that $k_1 \leqslant 0$ and $k_2, k_3 \geqslant 0$. This simple observation allows the following manipulation:

$$\max_{\substack{(k_1,k_2,k_3)\in[-\pi n,\pi n]^3 \\ \sum_{i=1}^{3} k_i = 0}} \{-2t\cos k_1 - 2t\cos k_2 - 2t\cos k_3\} = \max_{-\pi n \leqslant k_1 \leqslant 0} \{-2t\cos k_1 + \max_{0 \leqslant k_2 \leqslant -k_1} \{-2t\cos k_2 - 2t\cos(k_1 + k_2)\}\}. \quad \text{(A1)}$$

Since $\max_{0\leqslant k_2\leqslant -k_1}\{-2t\cos k_2 - 2t\cos(k_1 + k_2)\}$ is achieved by choosing $k_2 = 0$ (or equivalently $k_2 = -k_1$), we are left with the problem of finding

$$\max_{-\pi n \leqslant k_1 \leqslant 0} \{-4t\cos k_1\} - 2t, \quad \text{(A2)}$$

which manifestly leads to the optimal value $k_1 = -\pi n$. The third momentum value is obtained from the constraint $k_3 = -k_1 - k_2 = \pi n$ (or equivalently $k_3 = 0$ after the alternative choice $k_2 = -k_1$), thus confirming the aforementioned optimal choice.

This observation motivates the form of the BCS-like wave function proposed in Eq. (3) of the main text. As the reader can observe, the creation of a trimer at momentum k is accompanied in the variational ansatz by the annihilation of three fermions at momenta k and $\sim \pm\,(k_F - 2|k|)$, so that the identified most prominent correlation effects between the two fluids are qualitatively taken into account while preserving the analytical tractability of the trial wave function.

2. The variational ansatz $|\Psi_3\rangle$

The introduction of δ_k in the definition of the variational wave function $|\Psi_3\rangle$ is justified by following the thinking process leading to Eq. (3) of the main text. Indeed, we want to construct a state that gradually interpolates between a Fermi sea of fermions occupying momenta $-k_F < k < k_F$ and a Fermi sea of trimers occupying momenta $-\frac{k_F}{3} < k < \frac{k_F}{3}$ by means of the most relevant correlation effects between the two species. As the above calculation suggests, the latter are given

by recombination processes where the creation of a trimer at momentum $k \in (-\frac{k_F}{3}, \frac{k_F}{3})$ is accompanied by the annihilation of fermions at momenta $-k_F + A|k|$, k, $k_F - A|k|$, A being a proportionality constant.

By imposing that the filling of the entire Fermi sea of trimers must correspond to the full depletion of the Fermi sea of fermions, one easily notices that it implies $A = 2$. However, this condition alone is not sufficient for two reasons: (i) the fermionic states at momenta $\pm(k_F - 2|k| + \frac{2\pi}{L})$ (i.e., separated by an odd number of momentum quantization steps from k_F) are not getting depleted and (ii) the fermionic momenta getting depleted while filling trimer states at momenta k and $-k$ coincide, thus hindering the analytical tractability of an ansatz in the form of $|\Psi_3\rangle$. We solve these issues by depleting the momenta of the form $\pm(k_F - 2|k| + \frac{2\pi}{L})$ when filling the $k < 0$ trimer states, relying on the fact that a shift of $\frac{2\pi}{L}$ in the chosen momenta will not impact the qualitative features of the results in the thermodynamic limit.

3. Expression for the energy density and optimal variational parameters

As discussed in the main text, when the bands of fermions and trimers have both their minima at $k = 0$, we need to enrich the noninteracting two-fluid model with an interspecies coupling term in order to take recombination processes into account.

The two-fluid model including an interaction term between fermions and trimers reads

$$\hat{H}_{2\mathrm{F}} = \sum_k (\epsilon_{k,f} - \mu)\hat{a}_k^\dagger \hat{a}_k + \sum_k (\epsilon_{k,t} - 3\mu)\hat{d}_k^\dagger \hat{d}_k + \frac{ig}{3L}\sum_{k_1,k_2,k_3} f(k_1,k_2,k_3)\hat{d}_{k_1+k_2+k_3}^\dagger \hat{a}_{k_1}\hat{a}_{k_2}\hat{a}_{k_3} + \mathrm{H.c.}, \tag{A3}$$

where the last term is the reciprocal space representation of

$$\hat{H}_{\mathrm{int}} = g\sum_j \hat{d}_j^\dagger \hat{a}_{j-1}\hat{a}_j\hat{a}_{j+1} + \mathrm{H.c.} \tag{A4}$$

and $f(k_1,k_2,k_3) = \sin(k_3 - k_1) + \sin(k_2 - k_3) + \sin(k_1 - k_2)$.

The evaluation of the expectation value of the energy over the variational state $|\Psi_3\rangle$ gives as a result:

$$\begin{aligned}\langle \hat{H}_{2\mathrm{F}}\rangle_{\Psi_3} - E_{FS} = &\sum_{0\leqslant k<\frac{k_F}{3}} \left[(\epsilon_{k,t} - \epsilon_{k,F} - \epsilon_{k_F-2k,F} - \epsilon_{-k_F+2k,F})|\beta_k|^2 + \frac{4g}{L} f(k, k_F - 2k, -k_F + 2k)\mathrm{Im}\{\alpha_k^*\beta_k\}\right] \\ &+ \sum_{-\frac{k_F}{3}<k<0} \left[(\epsilon_{k,t} - \epsilon_{k,F} - \epsilon_{k_F+2k+\frac{2\pi}{L},F} - \epsilon_{-k_F-2k-\frac{2\pi}{L},F})|\beta_k|^2\right. \\ &\left. + \frac{4g}{L} f\left(k, k_F + 2k + \frac{2\pi}{L}, -k_F - 2k - \frac{2\pi}{L}\right)\mathrm{Im}\{\alpha_k^*\beta_k\}\right],\end{aligned} \tag{A5}$$

where E_{FS} is the energy of the fermionic Fermi sea filled up to the Fermi momentum k_F.

At this point we perform the following approximations: (i) we plug in the expressions $\epsilon_{k,F} = -2t\cos k$ and $\epsilon_{k,t} = -2t'\cos k$ for the noninteracting dispersion relations of fermions and trimers; (ii) due to the normalization condition, we parametrize the unknown coefficients as $\alpha_k = \cos\theta_k$, $\beta_k = e^{i\varphi_k}\sin\theta_k$, as detailed in the main text; (iii) assuming that the system size L is sufficiently large, we perform the replacement $\sum_k \to \frac{L}{2\pi}\int dk$, we neglect the shifts by $\frac{2\pi}{L}$ and we change variable according to $k \to -k$ in the resulting integral ranging over negative values of k; as a result one obtains Eq. (4) of the main text.

The expression in Eq. (4) of the main text is a functional of the variational parameters θ_k and ϕ_k, but it is trivial, as it does not feature terms coupling the unknown functions θ_k and ϕ_k in a nonlocal way. Thus, its minimization boils down to the minimization of the integrand function with respect to the two variables θ_k and ϕ_k for each value of k separately. A standard calculation leads to the optimal values displayed in Eq. (6) of the main text.

The value of the optimal parameters depends crucially on the sign of A_k. Therefore, we plot in Fig. 9 the function A_k in the interval $0 \leqslant k \leqslant k_F/3$ in three cases, representing, respectively, the small τ, intermediate τ, and large τ behavior of A_k. We observe that a small value of τ, where we expect to predict the F phase, is linked to a strictly positive A_k profile, while a large value of τ, where the T_0 phase is supposed to appear, is associated with a strictly negative A_k profile.

In an intermediate regime of τ values, instead, A_k changes sign at a value of $k \in [0, k_F/3]$ that continuously grows from $k = 0$ to $k = k_F/3$. The boundaries of the interval of τ values where this happens are found by determining the values τ_1 and τ_2 of τ such that $A_{k=0}$ and $A_{k=k_F/3}$ vanish, respectively. The result reads

$$\begin{aligned}\tau_1 &= 1 + 2\cos(\pi n), \\ \tau_2 &= 3.\end{aligned} \tag{A6}$$

4. Behavior of the trimer density

In order to properly identify the phases predicted by the variational ansatz, we compute the trimer

density as a function of τ in the thermodynamic limit. The expression of this observable is easily written as

$$n_T = \frac{1}{L}\sum_k \langle \hat{d}_k^\dagger \hat{d}_k \rangle = \frac{1}{\pi}\int_0^{\frac{k_F}{3}} dk \sin^2\theta_k. \tag{A7}$$

Since in the thermodynamic limit $\theta_k = \frac{\pi}{2}\Theta[-A(k)]$ because $B_k \propto L^{-1}$, the evaluation of n_T becomes trivial. In particular, when $\tau < \tau_1$ one has a strictly positive $A(k)$ profile, which implies $\theta_k = 0$ and thus $n_T = 0$. Thus, we identify this regime with the F phase. In a similar manner, since $A(k)$ is strictly negative when $\tau > \tau_2$, we get $\theta_k = \frac{\pi}{2}$, which results in $n_T = n/3$. We link this result with the T_0 phase. Finally, when $\tau_1 < \tau < \tau_2$, one has $A(k) < 0$ for $0 < k < K(\tau)$ and $A(k) > 0$ for $K(\tau) < k < k_F/3$, where $K(\tau)$ denotes the intermediate zero of $A(k)$ as a function of τ. In this case, the trimer density takes the form

$$\begin{aligned} n_T &= \frac{1}{\pi}\left(\int_0^{K(\tau)} dk \sin^2\theta_k + \int_{K(\tau)}^{\frac{k_F}{3}} dk \sin^2\theta_k\right) \\ &= \frac{1}{\pi}\int_0^{K(\tau)} dk = \frac{K(\tau)}{\pi}. \end{aligned} \tag{A8}$$

Hence, the trimer density takes an intermediate value $0 < n_T < n/3$, which implies that the fermionic density $n_F = n - 3n_T$ is nonvanishing as well and the two species coexist, as expected for a TF-H phase. Equation (A8) forces the interpretation of the zero of $A(k)$ as the Fermi momentum of the trimer Fermi sea as a function of τ.

5. Critical behavior of the energy density

The behavior of the energy density in the thermodynamic limit can be as well evaluated in the three phases. We assume in the following that the g does not scale extensively as the system size.

In the F phase, $A_k > 0 \ \forall k \in [0, \pi n/3]$, implying that $\theta_k = \frac{1}{2}\arctan(\frac{2B_k}{A_k})$ and therefore resulting in the optimal energy:

$$\frac{\langle \hat{H}_{2\mathrm{F}}\rangle_{\Psi_3} - E_{FS}}{Lt} = 2\int_0^{\frac{k_F}{3}} \frac{dk}{2\pi}\left\{A_k \sin^2\left[\frac{1}{2}\arctan\left(\frac{2B_k}{A_k}\right)\right] - B_k \sin\left[\arctan\left(\frac{2B_k}{A_k}\right)\right]\right\}. \tag{A9}$$

As $L \to +\infty$, $B_k \propto L^{-1}$ vanishes and therefore

$$\lim_{L\to+\infty} \frac{\langle \hat{H}_{2\mathrm{F}}\rangle_{\Psi_3} - E_{FS}}{Lt} = 0, \tag{A10}$$

indicating that the energy of the system equals the energy of the fermionic Fermi sea.

In the T_0 phase, instead, one has $A_k < 0 \ \forall k \in [0, \pi n/3]$, which implies that $\theta_k = \frac{1}{2}\arctan(\frac{2B_k}{A_k}) + \frac{\pi}{2}$ and gives as a result the optimal energy:

$$\frac{\langle \hat{H}_{2\mathrm{F}}\rangle_{\Psi_3} - E_{FS}}{Lt} = 2\int_0^{\frac{k_F}{3}} \frac{dk}{2\pi}\left\{A_k \sin^2\left[\frac{\pi}{2} + \frac{1}{2}\arctan\left(\frac{2B_k}{A_k}\right)\right] - B_k \sin\left[\pi + \arctan\left(\frac{2B_k}{A_k}\right)\right]\right\}. \tag{A11}$$

As $L \to +\infty$, the second term clearly vanishes, as it is bounded from above by an expression proportional to L^{-1}, while the first term converges to A_k and gives

$$\lim_{L\to+\infty} \frac{\langle \hat{H}_{2\mathrm{F}}\rangle_{\Psi_3} - E_{FS}}{Lt} = \frac{1}{\pi}\int_0^{\frac{k_F}{3}} A_k = -\frac{2}{\pi}\left(\tau - \frac{\sin(\pi n)}{\sin\left(\frac{\pi n}{3}\right)}\right)\sin\left(\frac{\pi n}{3}\right). \tag{A12}$$

In the intermediate regime $\tau_1 < \tau < \tau_2$, one has that $A_k < 0 \ \forall k \in [0, K(\tau))$ and $A_k > 0 \ \forall k \in (K(\tau), \pi n/3]$; therefore, the optimal energy takes the form

$$\begin{aligned} \frac{\langle \hat{H}_{2\mathrm{F}}\rangle_{\Psi_3} - E_{FS}}{Lt} = {} & 2\int_0^{K(\tau)} \frac{dk}{2\pi}\left\{A_k \sin^2\left[\frac{\pi}{2} + \frac{1}{2}\arctan\left(\frac{2B_k}{A_k}\right)\right] - B_k \sin\left[\pi + \arctan\left(\frac{2B_k}{A_k}\right)\right]\right\} \\ & + 2\int_{K(\tau)}^{\frac{k_F}{3}} \frac{dk}{2\pi}\left\{A_k \sin^2\left[\frac{1}{2}\arctan\left(\frac{2B_k}{A_k}\right)\right] - B_k \sin\left[\arctan\left(\frac{2B_k}{A_k}\right)\right]\right\}. \end{aligned} \tag{A13}$$

The second term goes to zero in the large size limit, while the first term gives

$$\lim_{L\to+\infty} \frac{\langle \hat{H}_{2\mathrm{F}}\rangle_{\Psi_3} - E_{FS}}{Lt} = \frac{1}{\pi}\int_0^{K(\tau)} A_k = \frac{2}{\pi}(1-\tau)\sin K(\tau) + \frac{2}{\pi}\sin(\pi n) - \frac{2}{\pi}\sin[\pi n - 2K(\tau)]. \tag{A14}$$

The asymptotic behavior of the energy as it approaches the critical points can then be obtained by deriving the one of the zero $K(\tau)$ when τ is close to either of the critical points; the latter is found by expanding the condition $A(k) = 0$ around $k = 0$ and $k = \frac{\pi n}{3}$, obtaining

$$K(\tau) \sim \frac{\tau - \tau_1}{4\sin(\pi n)} \quad \text{and} \quad K(\tau) \sim \frac{\pi n}{3} - \frac{1}{6}\cot\left(\frac{\pi n}{3}\right)(\tau_2 - \tau). \tag{A15}$$

As a result, in the limit $\tau \to \tau_1^+$, the energy density behaves as

$$\frac{\langle \hat{H}_{2F}\rangle_{\Psi_3} - E_{FS}}{Lt} \approx -\frac{(\tau-\tau_1)^2}{4\pi \sin(\pi n)}, \tag{A16}$$

while in the limit $\tau \to \tau_2^-$, the energy density behaves as

$$\frac{\langle \hat{H}_{2F}\rangle_{\Psi_3} - E_{FS}}{Lt} \approx \frac{2}{\pi}\sin(\pi n) - \frac{6}{\pi}\sin\left(\frac{\pi n}{3}\right) + \frac{2}{\pi}\sin\left(\frac{\pi n}{3}\right)(\tau_2-\tau) - \frac{1}{6\pi}\frac{\cos^2\left(\frac{\pi n}{3}\right)}{\sin\left(\frac{\pi n}{3}\right)}(\tau_2-\tau)^2. \tag{A17}$$

Hence, we recover the finite jump discontinuities in the second derivative associated with the appearance/disappearance of a gapless mode when entering/exiting a coexistence phase of fermions and trimers, as expected from the vanishing of the interspecies interaction energy in the thermodynamic limit.

We remark that the assumption that $g = O(1)$ is crucial in deriving the results above. As shown in Fig. 3 of the main text, the predictions of the 3BCS model replicate in a reliable manner the features of the DMRG data as for qualitative aspects of the energy first derivative and its scaling with L. Nevertheless, the numerical data do not show undisputedly the critical behavior predicted by the 3BCS model and thus we are unable to rule out with absolute certainty a different kind of criticality separating the F phase from the TF-H phase.

6. Occupation functions

We characterize here the behavior of the fermionic occupation function $n_F(k) = \langle \hat{a}_k^\dagger \hat{a}_k \rangle$ and of the trimer occupation function $n_T(k) = \langle \hat{d}_k^\dagger \hat{d}_k \rangle$. The fermionic occupation function takes the form

$$n_F(k) = \begin{cases} \cos^2\theta_{|k|}, & |k| < \frac{k_F}{3}, \\ \cos^2\theta_{\frac{k_F-|k|}{2}}, & \frac{k_F}{3} < |k| < k_F, \end{cases} \tag{A18}$$

whereas the trimer occupation function reads

$$n_T(k) = \sin^2\theta_{|k|}, \quad |k| < \frac{k_F}{3}. \tag{A19}$$

Thus, in the thermodynamic limit we can identify the functions $n_F(k)$ and $n_T(k)$ in the three phases of the model, as shown in Figs. 10(a)–10(d): in the F phase, $\theta_k = 0$ for every value of k and $n_F(k) = \mathbf{1}_{[-k_F,k_F]}(k)$, recovering the standard Fermi sea filled up to momentum k_F, while $n_T(k)$ vanishes; in the TF-H phase, $\theta_k = \frac{\pi}{2}$ for $0 < k < K(\tau)$ and $\theta_k = 0$ for $K(\tau) < k < \frac{k_F}{3}$, and therefore one gets $n_F(k) = \mathbf{1}_{[-k_F+2K(\tau),K(\tau)]\cup[K(\tau),k_F-2K(\tau)]}(k)$ and $n_T(k) = \mathbf{1}_{[-K(\tau),K(\tau)]}(k)$ (recovering the qualitative structure of the numerical data in Fig. 4 of the main text); in the T_0 phase, instead, $\theta_k = \frac{\pi}{2}$ for every value of k, resulting in a vanishing $n_F(k)$ and $n_T(k) = \mathbf{1}_{[-k_F/3,k_F/3]}(k)$, i.e., a Fermi sea of trimers at density $\frac{n}{3}$.

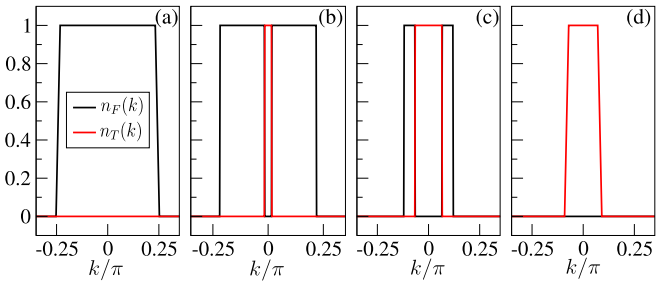

FIG. 10. Occupation functions $n_F(k)$ and $n_T(k)$ in the thermodynamic limit in the (a) F phase for $\tau = 2.0$, (b) TF-C phase for $\tau = 2.55$, (c) TF-C phase for $\tau = 2.9$, and (d) T_0 phase for $\tau = 3.1$.

7. Finite size effects from the variational energy density

The variational expression of Eq. (4) of the main text for the energy density holds in the limit of large sizes, as it was constructed by replacing discrete sums over momenta with continuous integrals via the rule $\sum_k \to \frac{L}{2\pi}\int dk$. If we take the thermodynamic limit of the 3BCS model, the ratio g/L tends to zero and the minimization of the energy functional becomes particularly simple: φ_k is unconstrained and θ_k takes only two values: 0 when $A_k > 0$ and $\pi/2$ when $A_k < 0$. Thus, for each value of k, either $\alpha_k = 1$, $\beta_k = 0$ or vice versa, and the ansatz becomes a product state in momentum space, i.e., an uncorrelated state of delocalized fermions and trimers.

Therefore, we need to clearly identify which finite size effects are induced by the presence of a nonvanishing value of $\frac{g}{Lt}$ and which ones appear as a result of a small value of L. The answer to this question is presented in Figs. 11(a) and 11(b), where the profile of the first derivative of the variational ground state energy density is shown for different choices of L and g. When the value of L is within reach of numerical simulations but not necessarily sufficient to display clear thermodynamic limit behavior [Fig. 11(a)], the comparison between the curves corresponding to different values of hybridization proves that trimer-fermion coupling smoothens out the profile around the critical point separating the F phase

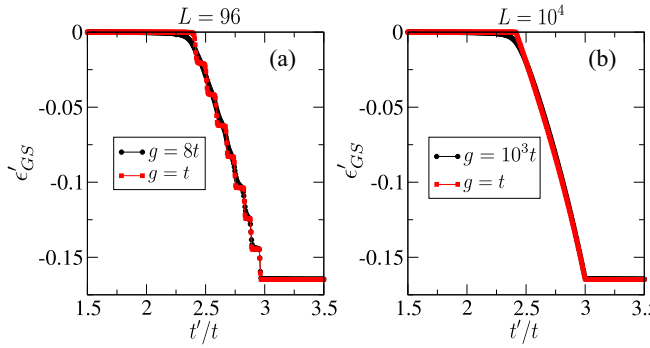

FIG. 11. (a) First derivative of the energy density with respect to t'/t within our BCS-like approach for $g = t$, $8t$ and $L = 96$. (b) First derivative of the energy density with respect to t'/t within our BCS-like approach for $g = t$, $10^3 t$ and $L = 10^4$.

from the TF-H phase; on the other hand, the steplike behavior of the curves for $L = 96$ is present irrespectively of the value of g and is purely a finite-size effect, as it disappears from the plots displayed in Fig. 11(b) for $L = 10^4$. Furthermore, the effect of a sufficiently large value of g relative to Lt replicates the phenomenology observed at finite size, thus confirming the aforementioned conclusion on the effect of the interspecies coupling g.

[1] H.-W. Hammer and L. Platter, Annu. Rev. Nucl. Part. Sci. **60**, 207 (2010).
[2] E. Braaten and H.-W. Hammer, Ann. Phys. **322**, 120 (2007), January Special Issue 2007.
[3] P. Schuck *et al.*, Phys. Scr. **91**, 123001 (2016).
[4] X.-W. Guan, M. T. Batchelor, and C. Lee, Rev. Mod. Phys. **85**, 1633 (2013).
[5] V. N. Efimov, Yadern. Fiz. **12**, 1080 (1970).
[6] V. Efimov, Nucl. Phys. A **210**, 157 (1973).
[7] D. S. Petrov, Phys. Rev. A **67**, 010703(R) (2003).
[8] S. Piatecki and W. Krauth, Nat. Commun. **5**, 3503 (2014).
[9] J. Carlson, S. Gandolfi, U. van Kolck, and S. A. Vitiello, Phys. Rev. Lett. **119**, 223002 (2017).
[10] M. Kunitski *et al.*, Science **348**, 551 (2015).
[11] E. Kolganova, A. Motovilov, and W. Sandhas, Few-Body Syst. **58**, 35 (2017).
[12] A. Rapp, G. Zaránd, C. Honerkamp, and W. Hofstetter, Phys. Rev. Lett. **98**, 160405 (2007).
[13] S. Capponi, G. Roux, P. Lecheminant, P. Azaria, E. Boulat, and S. R. White, Phys. Rev. A **77**, 013624 (2008).
[14] P. Lecheminant *et al.*, Int. J. Mod. Phys. E **17**, 2110 (2008).
[15] X. W. Guan, M. T. Batchelor, C. Lee, and J. Y. Lee, Europhys. Lett. **86**, 50003 (2009).
[16] P. Azaria, S. Capponi, and P. Lecheminant, Phys. Rev. A **80**, 041604(R) (2009).
[17] S. Backes, I. Titvinidze, A. Privitera, and W. Hofstetter, Phys. Rev. A **86**, 013633 (2012).
[18] P. Niemann and H.-W. Hammer, Phys. Rev. A **86**, 013628 (2012).
[19] J. Pohlmann, A. Privitera, I. Titvinidze, and W. Hofstetter, Phys. Rev. A **87**, 023617 (2013).
[20] P. E. Kornilovitch, Europhys. Lett. **103**, 27005 (2013).
[21] C. C. N. Kuhn and A. Foerster, New J. Phys. **14**, 013008 (2012).
[22] P. He, Y. Jiang, X. Guan, and J. He, J. Phys. A: Math. Theor. **48**, 015002 (2015).
[23] E. Szirmai, G. Barcza, J. Sólyom, and O. Legeza, Phys. Rev. A **95**, 013610 (2017).
[24] E. Burovski, G. Orso, and T. Jolicoeur, Phys. Rev. Lett. **103**, 215301 (2009).
[25] G. Orso, E. Burovski, and T. Jolicoeur, Phys. Rev. Lett. **104**, 065301 (2010).
[26] G. Roux, E. Burovski, and T. Jolicoeur, Phys. Rev. A **83**, 053618 (2011).
[27] T. Keilmann, I. Cirac, and T. Roscilde, Phys. Rev. Lett. **102**, 255304 (2009).
[28] M. Dalmonte, K. Dieckmann, T. Roscilde, C. Hartl, A. E. Feiguin, U. Schollwock, and F. Heidrich-Meisner, Phys. Rev. A **85**, 063608 (2012).
[29] W. Zhang, R. Li, W. X. Zhang, C. B. Duan, and T. C. Scott, Phys. Rev. A **90**, 033622 (2014).
[30] E.-N. Fan, T. C. Scott, and W.-Z. Zhang, Chinese Phys. B **26**, 043701 (2017).
[31] Y.-Z. You, Z. Chen, X.-Q. Sun, and H. Zhai, Phys. Rev. Lett. **109**, 265302 (2012).
[32] W. Zhang, Y. Yang, L. Guo, C. Ding, and T. C. Scott, Phys. Rev. A **91**, 033613 (2015).
[33] G. Guijarro, G. E. Astrakharchik, J. Boronat, B. Bazak, and D. S. Petrov, Phys. Rev. A **101**, 041602(R) (2020).
[34] S. Musolino, H. Kurkjian, M. VanRegemortel, M. Wouters, S. J. J. M. F. Kokkelmans, and V. E. Colussi, Phys. Rev. Lett. **128**, 020401 (2022).
[35] N. Read and E. Rezayi, Phys. Rev. B **59**, 8084 (1999).
[36] G. Moore and N. Read, Nucl. Phys. B **360**, 362 (1991).
[37] N. Read and D. Green, Phys. Rev. B **61**, 10267 (2000).
[38] A. Y. Kitaev, Phys. Usp. **44**, 131 (2001).
[39] M. Mattioli, M. Dalmonte, W. Lechner, and G. Pupillo, Phys. Rev. Lett. **111**, 165302 (2013).
[40] M. Dalmonte, W. Lechner, Z. Cai, M. Mattioli, A. M. Lauchli, and G. Pupillo, Phys. Rev. B **92**, 045106 (2015).
[41] J. Ruhman and E. Altman, Phys. Rev. B **96**, 085133 (2017).
[42] C. L. Kane, A. Stern, and B. I. Halperin, Phys. Rev. X **7**, 031009 (2017).
[43] Y. He, B. Tian, D. Pekker, and R. S. K. Mong, Phys. Rev. B **100**, 201101(R) (2019).
[44] L. Gotta, L. Mazza, P. Simon, and G. Roux, Phys. Rev. Research **3**, 013114 (2021).
[45] L. Gotta, L. Mazza, P. Simon, and G. Roux, Phys. Rev. Lett. **126**, 206805(2021).
[46] L. Gotta, L. Mazza, P. Simon, and G. Roux, Phys. Rev. B **104**, 094521(2021).
[47] L. Mazza, F. Iemini, M. Dalmonte, and C. Mora, Phys. Rev. B **98**, 201109(R) (2018).
[48] S. R. White, Phys. Rev. Lett. **69**, 2863 (1992).
[49] S. R. White, Phys. Rev. B **48**, 10345 (1993).
[50] U. Schollwöck, Rev. Mod. Phys. **77**, 259 (2005).
[51] U. Schollwöck, Ann. Phys. **326**, 96 (2011).
[52] M. Fishman, S. R. White, and E. M. Stoudenmire, arXiv:2007.14822.